

The Importance of Satellite Quenching for the Build-Up of the Red Sequence of Present Day Galaxies

Frank C. van den Bosch^{1*}, Daniel Aquino¹, Xiaohu Yang², H.J. Mo³,
Anna Pasquali¹, Daniel H. McIntosh³, Simone M. Weinmann⁴, Xi Kang¹

¹*Max-Planck-Institute for Astronomy, Königstuhl 17, D-69117 Heidelberg, Germany*

²*Shanghai Astronomical Observatory; the Partner Group of MPA, Nandan Road 80, Shanghai 200030, China*

³*Department of Astronomy, University of Massachusetts, Amherst MA 01003-9305, USA*

⁴*Institute for Theoretical Physics, University of Zurich, CH-8057, Zurich, Switzerland*

ABSTRACT

According to the current paradigm, galaxies initially form as disk galaxies at the centers of their own dark matter haloes. During their subsequent evolution they may undergo a transformation to a red, early-type galaxy, thus giving rise to the build-up of the red sequence. Two important, outstanding questions are (i) which transformation mechanisms are most important, and (ii) in what environment do they occur. In this paper we study the impact of transformation mechanisms that operate only on satellite galaxies, such as strangulation, ram-pressure stripping and galaxy harassment. Using a large galaxy group catalogue constructed from the Sloan Digital Sky Survey, we compare the colors and concentrations of satellite galaxies to those of central galaxies of the same stellar mass, adopting the hypothesis that the latter are the progenitors of the former. On average, satellite galaxies are redder and more concentrated than central galaxies of the same stellar mass, indicating that satellite specific transformation processes do indeed operate. Central-satellite pairs that are matched in both stellar mass and color, however, show no average concentration difference, indicating that the transformation mechanisms affect color more than morphology. We also find that the color and concentration differences of matched central-satellite pairs are completely independent of the halo mass of the satellite galaxy, indicating that satellite-specific transformation mechanisms are equally efficient in haloes of all masses. This strongly rules against mechanisms that are thought to operate only in very massive haloes, such as ram-pressure stripping or harassment. Instead, we argue that strangulation is the main transformation mechanism for satellite galaxies. Finally, we determine the relative importance of satellite quenching for the build-up of the red sequence. We find that roughly 70 percent of red sequence satellite galaxies with $M_* \sim 10^9 h^{-2} M_\odot$ had their star formation quenched as satellites. This drops rapidly with increasing stellar mass, reaching virtually zero at $M_* \sim 10^{11} h^{-2} M_\odot$. Therefore, a very significant fraction of red satellite galaxies were already quenched before they became a satellite.

Key words: galaxies: clusters: general – galaxies: haloes – galaxies: evolution – galaxies: general – galaxies: statistics – methods: statistical

1 INTRODUCTION

The local population of galaxies consists roughly of two types: early-types, which have a spheroidal morphology, are red, and have little or no ongoing star formation, and late-types, which have a disk morphology, are blue and have

active, ongoing star formation. In the current paradigm of galaxy formation, it is believed that virtually all galaxies initially form as late-type, disk galaxies due to the cooling of gas with non-zero angular momentum in virialized dark matter haloes. During the subsequent hierarchical evolution, these late-type galaxies are then transformed into early-types via a variety of mechanisms that cause morphological transformations and/or star formation quenching.

* E-mail: vdbosch@mpia.de

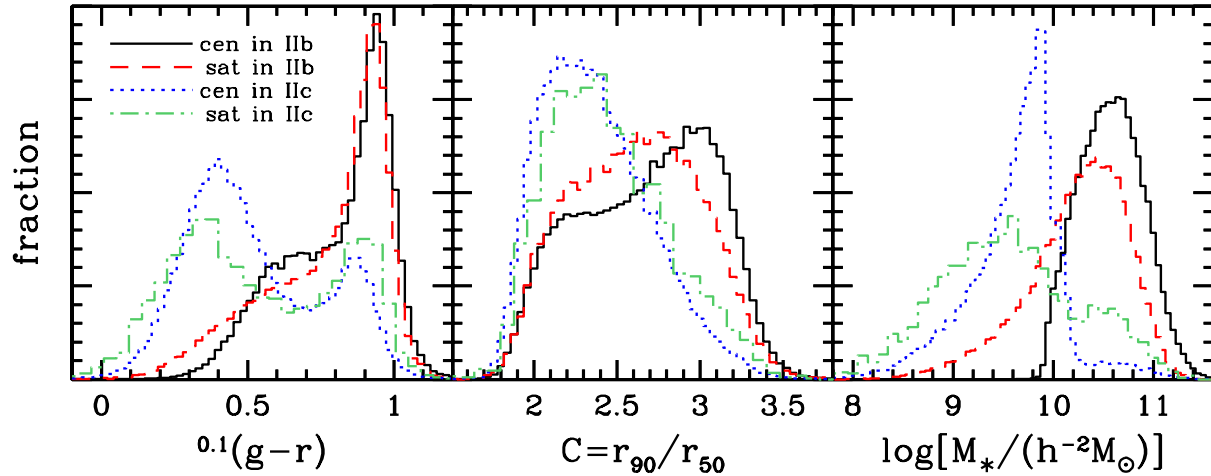


Figure 1. The distributions of color (left panel), concentration (middle panel) and stellar mass (right panel) of centrals and satellites in samples IIb and IIc, as indicated. Each individual distribution is normalized to unity; their relative normalizations can be inferred from Table 1.

Recent studies have shown that the bimodality of the galaxy population already exists at least out to $z \simeq 1$ (e.g., Bell et al. 2004; Tanaka et al. 2005; Cucciati et al. 2006; Cooper et al. 2006; Willmer et al. 2006), and that the total stellar mass density on the red sequence has roughly doubled over the last 6-8 Gyr (e.g., Bell et al. 2004; Borch et al. 2006; Zucca et al. 2006; Faber et al. 2007; Brown et al. 2007). This strongly supports the paradigm that galaxies initially form as disks and are subsequently transformed into early-types. What is still largely unknown, however, is what the dominant mechanisms are that cause the late- to early-type transition, and in what kind of environments they mainly operate.

A number of different mechanisms have been proposed. First of all, disk galaxies may be transformed into early-type spheroids during a major merger with another galaxy (e.g., Toomre & Toomre 1972; Negroponte & White 1983; Kauffmann, White & Guiderdoni 1993; Hopkins et al. 2006, 2007a,b). In order to ensure that the remnant remains a red, early-type galaxy, the merging scenario needs to be adjoined with a mechanism that can prevent any subsequent cooling and star formation following the merger, which would form a new disk and make the galaxy blue again. Currently, feedback from an active galactic nucleus (AGN) is believed to be the most promising mechanism that can accomplish this (e.g., Bower 2006; Croton et al. 2006; Kang, Jing & Silk 2006; Hopkins et al. 2006), though the details remain unclear. In addition to merging there are a number of transformation and quenching mechanisms which are special in that they only operate on satellite galaxies. When a small halo is accreted by a larger halo its hot, diffuse gas may be stripped thus removing its fuel for future star-formation (Larson, Tinsley & Caldwell 1980; Balogh, Navarro & Morris 2000). Following Balogh & Morris (2000) we refer to this process, that results in a fairly gradual decline of the satellite's star formation rate, as 'strangulation'. When the external pressure is sufficiently high, ram-pressure may also remove the cold gas of the satellite galaxy (e.g., Gunn & Gott 1972; Quilis, Moore & Bower 2000; Hester 2006a), resulting in an extremely fast quenching of its star formation.

In what follows we refer to the complete removal of the cold gas reservoir as 'ram-pressure stripping'. These two quenching mechanisms can transit blue satellite galaxies to the red sequence, but they do not have a (significant) impact on the overall morphology of the satellite galaxy. However, there are additional satellite-specific mechanisms that can transform disks into spheroids (or at least, result in more concentrated morphologies). Along its orbit a satellite galaxy is subject to tidal forces which may cause tidal stripping and heating. In addition, the morphologies of satellite galaxies can be strongly affected by the cumulative effect of many high speed (impulsive) encounters, a process called 'harassment' (Farouki & Shapiro 1981; Moore et al. 1996). Finally, although most mergers are believed to involve a central galaxy, satellite-satellite mergers do also occur (Makino & Hut 1997; Somerville & Primack 1999; McIntosh et al. 2007).

The goals of this paper are (i) to study the impact of these satellite-specific transformation mechanisms, (ii) to determine which process dominates, (iii) to determine the fraction of galaxies that undergo a transition from the blue sequence to the red sequence as satellites, and (iv) to investigate in what kind of environment these transitions take place. We use a large galaxy group catalogue constructed from the Sloan Digital Sky Survey (SDSS; York et al. 2000; Stoughton et al. 2002) by Yang et al. (2007). This group catalogue yields information regarding the halo mass in which each galaxy resides, and allows us to split the galaxy population into centrals and satellites. We use this catalogue to study how the properties of galaxies (in particular their color and concentration) change after they are accreted into a larger halo. We compare the properties of satellite galaxies with those of central galaxies of the same stellar mass, under the hypothesis that the latter are the progenitors of the former, in a statistical sense. We also examine what fraction of galaxies undergoes a transition from the blue sequence to the red sequence after having been accreted, by comparing the red fractions of centrals and satellites of the same stellar mass. Finally, we use the group catalogue to examine how the transformation efficiency depends on the mass of the halo into which a galaxy is accreted. All this information

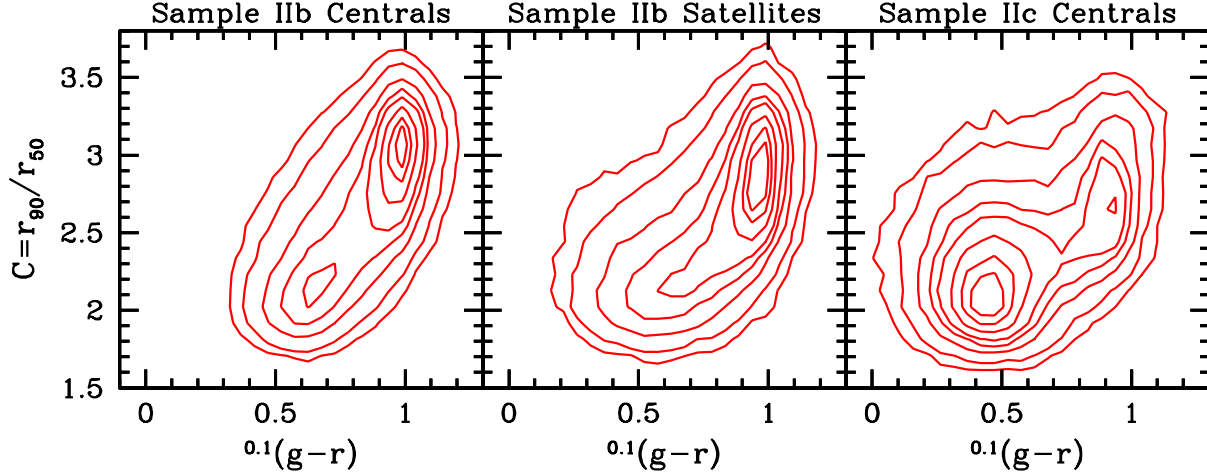


Figure 2. The distribution of galaxies in concentration-color space. Results are shown for centrals in sample IIb (left panel), satellites in sample IIb (middle panel) and centrals in sample IIc (right panel). Note that the fraction of blue, low concentration galaxies increases going from the left panel to the right panel, which mainly reflects a trend in stellar mass (cf. Fig. 1).

combined sheds important light on the efficiency with which the various satellite-specific transformation mechanisms discussed above operate.

Throughout this paper we adopt a flat Λ CDM cosmology with $\Omega_m = 0.238$ and $\Omega_\Lambda = 0.762$ (Spergel et al. 2007) and we express units that depend on the Hubble constant in terms of $h \equiv H_0/100 \text{ km s}^{-1} \text{ Mpc}^{-1}$. In addition, we use ‘log’ as shorthand for the 10-based logarithm.

2 DATA

The analysis presented in this paper is based on the SDSS DR4 galaxy group catalogue of Yang et al. (2007; hereafter Y07). This group catalogue is constructed applying the halo-based group finder of Yang et al. (2005a) to the New York University Value-Added Galaxy Catalogue (NYU-VAGC; see Blanton et al. 2005a), which is based on SDSS DR4 (Adelman-McCarthy et al. 2006). From this catalogue Y07 selected all galaxies in the Main Galaxy Sample with an extinction corrected apparent magnitude brighter than $m_r = 18$, with redshifts in the range $0.01 \leq z \leq 0.20$ and with a redshift completeness $C_z > 0.7$. This sample of galaxies is used to construct three group samples: sample I, which only uses the 362356 galaxies with measured redshifts from the SDSS, sample II which also includes 7091 galaxies with SDSS photometry but with redshifts taken from alternative surveys, and sample III which includes an additional 38672 galaxies that lack a redshift due to fiber-collisions, but which we assign the redshift of its nearest neighbor (cf. Zehavi et al. 2002). The present analysis is based on all galaxies in sample II with $m_r < 17.77$, which consists of 344348 galaxies, but we have checked that samples I and III give results that are almost indistinguishable.

The magnitudes and colors of all galaxies are based on the standard SDSS Petrosian technique (Petrosian 1976; Strauss et al. 2002), have been corrected for galactic extinction (Schlegel, Finkbeiner & Davis 1998), and have been K -corrected and evolution corrected to $z = 0.1$, using the method described in Blanton et al. (2003). Stellar masses for all galaxies are computed using the relations between stellar

Table 1. Galaxy Samples

ID	#gal	#grp	#cen	#sat	description
IIa	344348	281089	280879	63469	entire sample
IIb	278085	218282	218103	59982	with group mass
IIc	66263	62807	62776	3487	no group mass

Notes: Properties of the three galaxy samples used in this paper. Columns (2) to (5) list the numbers of galaxies, of groups, of central galaxies and of satellite galaxies, respectively. The sixth column gives a brief description of the sample. Sample IIa is the entire galaxy sample. Sample IIb consists of those galaxies for which the group has an assigned halo mass. Sample IIc consists of those galaxies for which the group does not have an assigned halo mass. Thus sample IIa is simply the sum of samples IIb and IIc.

mass-to-light ratio and color of Bell et al. (2003; see Appendix A). The main galaxy parameters that we use in this paper are the stellar mass, M_* , the $^{0.1}(g-r)$ color, and the concentration $C = r_{90}/r_{50}$. Here r_{90} and r_{50} are the radii that contain 90 and 50 percent of the Petrosian r -band flux, respectively. As shown by Strateva et al. (2001), C is a reasonable proxy for Hubble type, with $C > 2.6$ corresponding to an early-type morphology.

As described in Y07, the majority of the groups in our catalogue have two estimates of their dark matter halo mass M_h : one based on the ranking of its total characteristic luminosity, and the other based on the ranking of its total characteristic stellar mass. As shown in Y07, both halo masses agree very well with each other, with an average scatter that decreases from ~ 0.1 dex at the low mass end to ~ 0.05 dex at the massive end. In addition, detailed tests with mock galaxy redshift catalogues have demonstrated that these group masses are more reliable than those based on the velocity dispersion of the group members (Yang et al. 2005b; Weinmann et al. 2006a; Y07). In this paper we

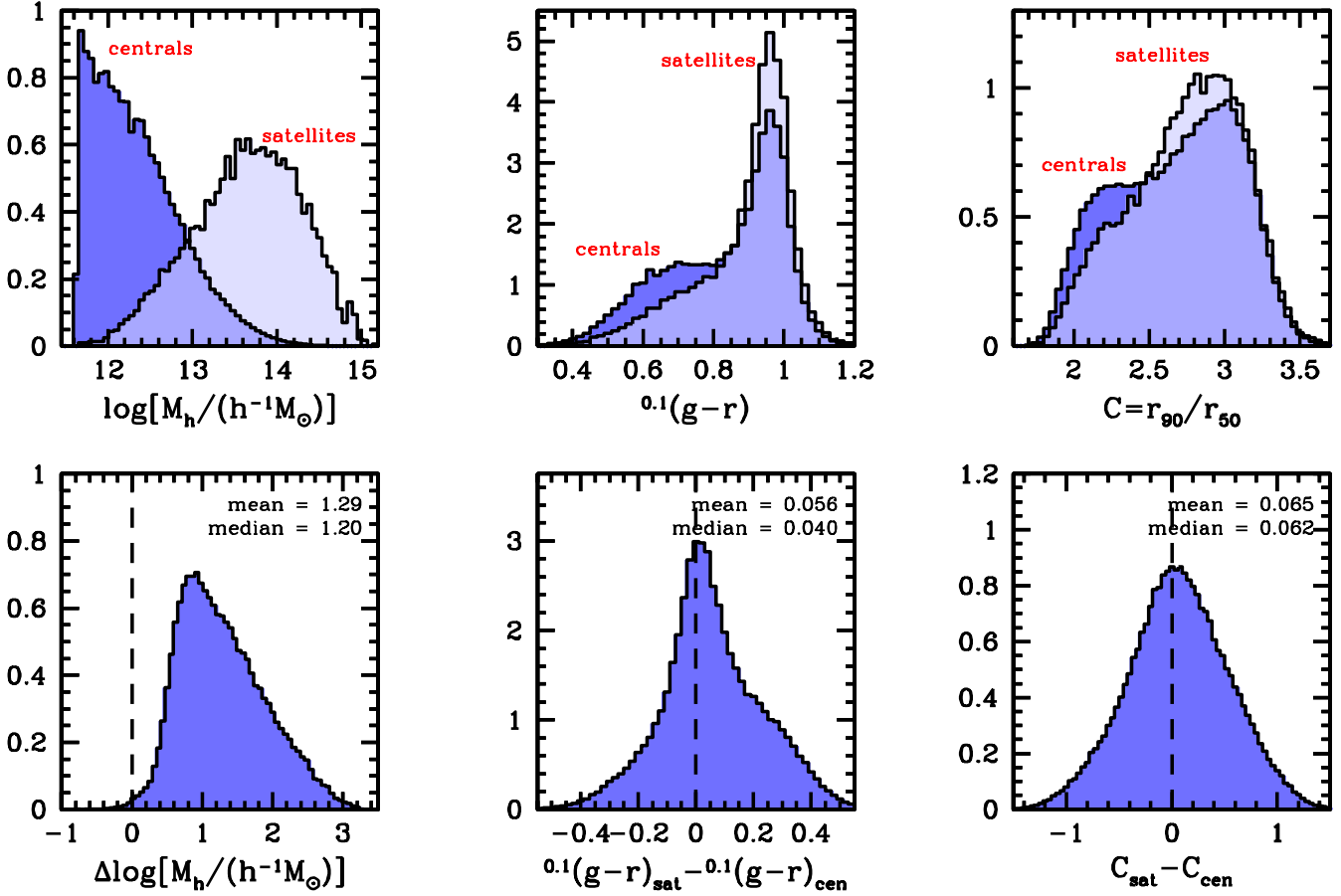


Figure 3. The upper left-hand panel shows the halo mass distributions of the central and satellite galaxies of sample IIb that are matched in stellar mass. The distributions for centrals and satellites are shaded dark and light, respectively, while an intermediate color is used to shade the overlap region. The lower left-hand panel shows the corresponding distribution of $\Delta \log M_h = M_{h,sat} - M_{h,cen}$, and shows that satellite galaxies live in haloes that are on average about one order of magnitude more massive than central galaxies of the same stellar mass. The middle and right-hand panels in the upper row show the color and concentration distributions, respectively, of the central galaxies (dark shading) and their matched satellites (light shading). Once again, an intermediate shading is used to indicate the overlap regions. Finally, the middle and right-hand panels of the lower row show the corresponding distributions of the color and concentration differences between centrals and their matched satellites. The mean and medians of both distributions are indicated.

adopt the group masses based on the stellar mass ranking[†]. These masses are available for a total of 218282 groups in our sample, which host a total of 278085 galaxies. This implies that a total of 66263 galaxies have been assigned to a group for which no reliable mass estimate is available.

2.1 Sample Definition and Global Properties

In this paper we consider three galaxy samples: sample IIa, which consists of all 344348 galaxies in group sample II with $m_r < 17.77$, sample IIb, which only considers the galaxies in groups that have an assigned mass, and sample IIc, which consists of the galaxies in groups that do not have an assigned mass. The properties of these three samples are listed in Table 1. In each sample we split the galaxies into “centrals”, which are the most massive group members in terms of their stellar mass, and “satellites”, which are those group

[†] We have verified, though, that none of our results change significantly if we adopt the luminosity-rank based masses instead.

members that are not centrals. Note that only 5.3 percent of the galaxies in sample IIc are satellites, compared to 18.4 and 21.6 percent in samples IIa and IIb, respectively.

Fig. 1 shows the (individually normalized) distributions of color, concentration, and stellar mass for central and satellite galaxies in samples IIb and IIc. Note that the color and concentration distributions of centrals and satellites in the same sample are remarkably similar, but that they are very different for different samples. In the case of sample IIb, both centrals and satellites reveal a pronounced red peak (representing red-sequence galaxies) and a modest blue tail. In the case of sample IIc, however, the color distribution has a much more pronounced blue peak and a less significant red-sequence, while the concentration distribution peaks at significantly lower values (again for both centrals and satellites). As is evident from the right-hand panel, galaxies in sample IIc have, on average, significantly lower stellar masses than galaxies in sample IIb. Another important difference between these two samples is the masses of the haloes in which the galaxies reside. More than 90 percent of the galaxies in sample IIb reside in haloes with

$M_h \geq 10^{11.8} h^{-1} M_\odot$. In the case of sample IIc, although no halo masses have been assigned to these galaxies, the majority almost certainly resides in low mass haloes with $M_h \lesssim 10^{12} h^{-1} M_\odot$. Therefore, Fig. 1 suggests that the colors and concentrations of a galaxy do not depend strongly on whether the galaxy is a central or a satellite, but are more closely related to their stellar mass or to the mass of their dark matter halo.

Fig. 2 shows the distribution of three galaxy samples in color-concentration space. Results are shown separately for central galaxies in sample IIb (left-hand panel), satellite galaxies in sample IIb (middle panel) and central galaxies in sample IIc (right-hand panel). There are clear differences: when moving from the left-hand panel to the right-hand panel, the fraction of blue galaxies with low concentrations increases profoundly. This confirms the conclusion reached above: if the main mechanism that determines whether a galaxy is an early-type (red and concentrated) or a late type (blue and less concentrated) is related to whether the galaxy is a central or a satellite, then the color-concentration distributions of the left- and right-hand panels should look similar, which is clearly not the case. On the other hand, the color-concentration distributions are consistent, at least quantitatively, with a picture in which the early-type fraction increases monotonically with stellar mass (cf. the right-hand panel of Fig. 1).

3 THE IMPACT OF SATELLITE QUENCHING

One of the main aims of this paper is to investigate to what extent the colors and concentrations of central galaxies change when they become a satellite galaxy (i.e., when they are accreted into a more massive halo). To this extent we compare the colors and concentrations of satellite galaxies to those of central galaxies of the same stellar mass, under the hypothesis that the latter are the progenitors of the former (in a statistical sense). We start by analyzing sample IIb, for which we have halo masses available. For each central galaxy in this sample we randomly pick a satellite galaxy whose stellar mass matches that of the central ($|\Delta \log M_*| \leq 0.01$) and we register the differences in color, $^{0.1}(g-r)_{\text{sat}} - ^{0.1}(g-r)_{\text{cen}}$, and concentration, $C_{\text{sat}} - C_{\text{cen}}$, as well as the masses of the haloes in which the central and satellite reside, $M_{h,\text{cen}}$ and $M_{h,\text{sat}}$, respectively. The upper left-hand panel of Fig. 3 shows the halo mass distributions of the centrals and satellites that are matched in stellar mass, while the lower left-hand panel shows the corresponding distribution of the differences, $\Delta \log M_h \equiv \log M_{h,\text{sat}} - \log M_{h,\text{cen}}$. Obviously satellite galaxies reside in more massive haloes than their central counterparts, with a mean $\Delta \log M_h$ of 1.29. Note that there are virtually no central-satellite pairs with $\Delta \log M_h < 0$. This is important since a central galaxy in a halo of mass M_h is not expected to ever become a satellite galaxy in a less massive halo. In other words, the fact that $\Delta \log M_h > 0$ for almost all of our matched central-satellite pairs is in line with the idea that centrals are the progenitors of satellites of the same stellar mass.

The middle and right-hand panels in the upper row of Fig. 3 show the color and concentration distributions of the centrals and their matched satellites. These are remarkably

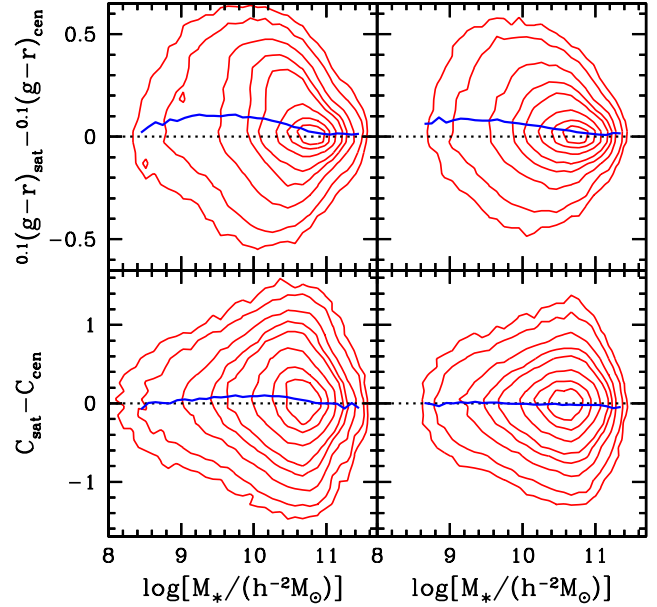


Figure 5. Contour plots of $^{0.1}(g-r)_{\text{sat}} - ^{0.1}(g-r)_{\text{cen}}$ (upper panels) and $C_{\text{sat}} - C_{\text{cen}}$ (lower panels) as functions of stellar mass for central-satellite pairs in Sample IIa. In the left-hand panels centrals and satellites have been matched in stellar mass only. In the right-hand panels they have been matched in stellar mass and concentration (upper-right panel) or in stellar mass and color (lower-right panel). Blue, solid lines indicate the running averages.

similar, though the satellites have a somewhat more pronounced red peak, and are more skewed towards higher concentrations. The middle panel in the lower row of Fig. 3 shows the distribution of the color differences between our matched central-satellite pairs. Although it is clearly skewed towards satellite galaxies being redder, the mean (median) of the distribution is only 0.056 (0.040). As is evident from a comparison with Figs. 1 and 2, this color difference is much smaller than the typical color difference between the red and blue sequences, which suggests that the fraction of satellite galaxies that undergoes a blue sequence to red sequence transition is relatively small (see §4). Finally, the lower right-hand panel of Fig. 3 shows the distribution of $C_{\text{sat}} - C_{\text{cen}}$ for our matched central-satellite pairs. This distribution is remarkably symmetric with a mean (median) of only 0.065 (0.062). Once again this difference is small compared to the variance in C shown in Figs. 1 and 2. This suggests that galaxies do not undergo a strong change in morphology once they become a satellite galaxy.

Fig. 4 plots the distribution of central-satellite pairs as function of both the color difference and the concentration difference. Results are shown for three bins in stellar mass, as indicated at the top of each panel, while we also indicate the percentage of pairs in each quadrant. For $10.0 < \log[M_*/(h^{-2} M_\odot)] < 10.5$ the distribution is clearly asymmetric with respect to the origin; almost half (43.9 percent) of all central-satellite pairs lie in the first quadrant (satellites are redder and more concentrated), compared to only 18.0 percent in the third quadrant (satellites are bluer and less concentrated). This clearly demonstrates that low mass galaxies undergo a significant transformation once they become a satellite galaxy. Also, the fact that the fourth

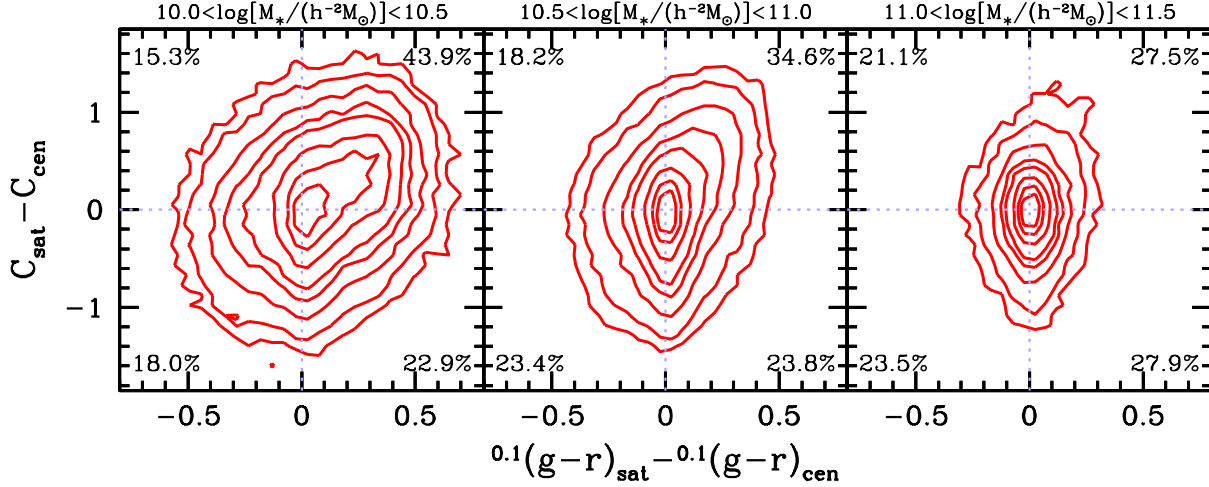


Figure 4. Contour plots of $0.1(g-r)_{\text{sat}} - 0.1(g-r)_{\text{cen}}$ versus $C_{\text{sat}} - C_{\text{cen}}$ for three bins in stellar mass (indicated at the top of each panel). The percentages of matched central-satellite pairs in each of the four quadrants are indicated.

quadrant contains a significantly larger fraction of galaxies than the second quadrant indicates that the transformation mechanism(s) have a larger impact on color than on concentration. Similar trends are apparent in the middle panel, corresponding to $10.5 < \log[M_*/(h^{-2} M_{\odot})] < 11.0$, albeit less pronounced. Finally, in the most massive bin (right-hand panel), the distribution starts to look remarkably symmetric, with only a very mild excess of pairs on the red side. Thus, there is a clear stellar mass dependence, in that less massive galaxies undergo a more pronounced transformation when they become a satellite galaxy.

Fig. 5 shows another rendition of this stellar mass dependence. It shows the distributions of $0.1(g-r)_{\text{sat}} - 0.1(g-r)_{\text{cen}}$ (upper panels) and $C_{\text{sat}} - C_{\text{cen}}$ (lower panels) as functions of stellar mass, with the blue, solid lines indicating the running averages. In order to maximize the dynamic range in stellar mass, we here use Sample IIa which includes galaxies in groups that lack an assigned halo mass (Sample IIb, though, yields similar results over the stellar mass range in common). Note that centrals with $M_* \gtrsim 10^{11} h^{-2} M_{\odot}$ have almost exactly the same colors and concentrations as satellite galaxies of the same stellar mass (on average). Towards lower M_* , however, the satellites become redder and more concentrated compared to a central galaxy of the same stellar mass. At $M_* \sim 10^{10} h^{-2} M_{\odot}$ satellites are, on average, ~ 0.1 magnitudes redder and have a concentration parameter that is ~ 0.1 larger than their central counterparts. Note also that there is a weak trend that the color and concentration differences become smaller again for $M_* \lesssim 3 \times 10^9 h^{-2} M_{\odot}$. In particular, centrals and satellites with $8 \lesssim \log[M_*/(h^{-2} M_{\odot})] \lesssim 9$ show no significant difference in concentration.

To a good approximation, ram-pressure stripping and strangulation should cause a change in color, but leave the concentration and stellar mass largely intact. Therefore, if either of these transformation mechanisms is efficient, we would expect satellite galaxies to be significantly redder than central galaxies of the same stellar mass *and the same concentration*. To test this we proceed as follows. For each central galaxy in sample IIa, we randomly pick a satellite galaxy whose stellar mass and concentration match that of

the central ($|\Delta \log M_*| \leq 0.01$ and $|\Delta C| \leq 0.01$), and we register the color difference. The upper right-hand panel of Fig. 5 shows the resulting distribution of the color differences as function of stellar mass. The running average is slightly smaller than in the case in which we only match the central-satellite pairs in stellar mass, though the differences are only modest. The lower right-hand panel of Fig. 5 shows the differences in concentration for central-satellite pairs matched in both stellar mass and color ($|\Delta \log M_*| \leq 0.01$ and $|\Delta 0.1(g-r)| \leq 0.01$). Remarkably, the running average is almost exactly zero over the entire range in stellar masses probed. This suggests that there are no satellite galaxies that undergo a change in concentration without a change in color. On the other hand, a significant fraction of satellite galaxies has undergone a change in color while maintaining the same concentration. This suggests that strangulation and/or ram-pressure stripping are more efficient than transformation mechanisms that affect morphology, such as harassment. It also nicely explains why broad-band colors are more predictive of environment than morphology, as noted by Hogg et al. (2003) and Blanton et al. (2005b), and is in good agreement with the results of Hester (2006b).

Having examined the stellar mass dependence, we now turn to the dependence on the halo mass of the satellite galaxy, $M_{\text{h,sat}}$. The left-hand panels of Fig. 6 show the color and concentration differences of central-satellite pairs in sample IIb that have been matched in stellar mass as functions of the halo mass of the satellite galaxy. The running averages are virtually independent of $M_{\text{h,sat}}$, but clearly offset from zero. This absence of any dependence on $M_{\text{h,sat}}$ suggests that the efficiency with which the transformation mechanisms operate are independent of halo mass. As we discuss in §5 this puts strong constraints on the viability of the various transformation mechanisms.

In the right-hand panels of Fig. 6 we repeat the same exercise, but this time we have matched the central-satellite pairs in both stellar mass and concentration (upper-right panel) or in both stellar mass and color (lower-right panel). Once again, there is no significant dependence on $M_{\text{h,sat}}$. Note also that, in agreement with the results shown in the lower-right panel of Fig. 5, centrals and satellites with the

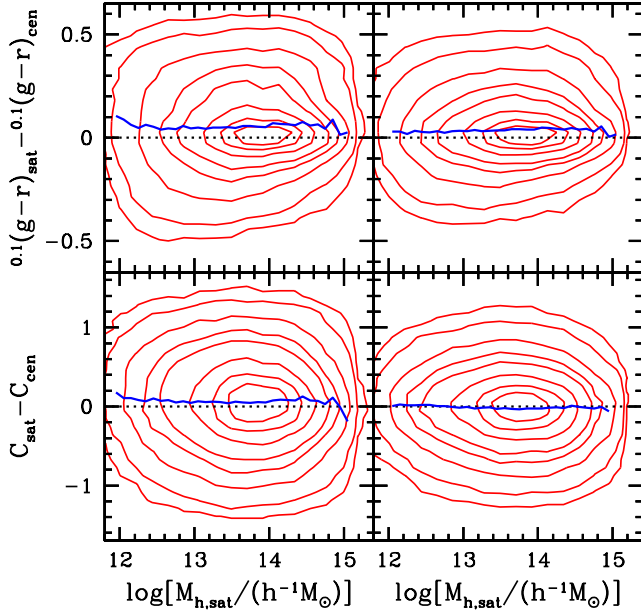


Figure 6. Contour plots of $0.1(g-r)_{\text{sat}} - 0.1(g-r)_{\text{cen}}$ (upper panels) and $C_{\text{sat}} - C_{\text{cen}}$ (lower panels) for central-satellite pairs in sample IIb as functions of the halo mass of the satellites. In the left-hand panels centrals and satellites have been matched in stellar mass only. In the right-hand panels they have been matched in stellar mass and concentration (upper-right panel) or in stellar mass and color (lower-right panel). Blue, solid lines indicate the running averages.

same stellar mass and the same color show no difference in concentration, on average.

4 TRANSITION FRACTIONS

Having determined the average differences in color and concentration between centrals and satellites of the same stellar mass, we now determine the *fractional* importance of satellite quenching for the build-up of the red sequence. We do this by comparing the red fractions of centrals and satellites. As a first step, we split our galaxy population in red and blue galaxies. Fig. 7 shows the color-stellar mass relation of all galaxies in sample IIa (centrals and satellites combined). Here we have weighted each galaxy by $1/V_{\text{max}}$, where V_{max} is the comoving volume of the Universe out to a comoving distance at which the galaxy would still have made the selection criteria of our sample. This weighting scheme corrects the sample for Malmquist bias, and for the fact that blue galaxies can be probed out to higher redshifts than red galaxies of the same stellar mass (see Appendix A). The color-stellar mass distribution clearly reveals the bimodality of the galaxy population: massive galaxies are mainly red, while low-mass galaxies are mainly blue. The red and blue lines in Fig. 7 delineate the red and blue sequences given by

$$0.1(g-r) = 0.1A + 0.15 (\log[M_*/(h^{-2} M_\odot)] - 10.0), \quad (1)$$

with $0.1A = 0.1A_{\text{red}} = 0.90$ and $0.1A = 0.1A_{\text{blue}} = 0.58$, respectively. These relations are simply fit by eye, and merely serve to illustrate the rough stellar mass dependence of the sequences. The dashed line indicates the color-cut adopted in this paper to split the population in red

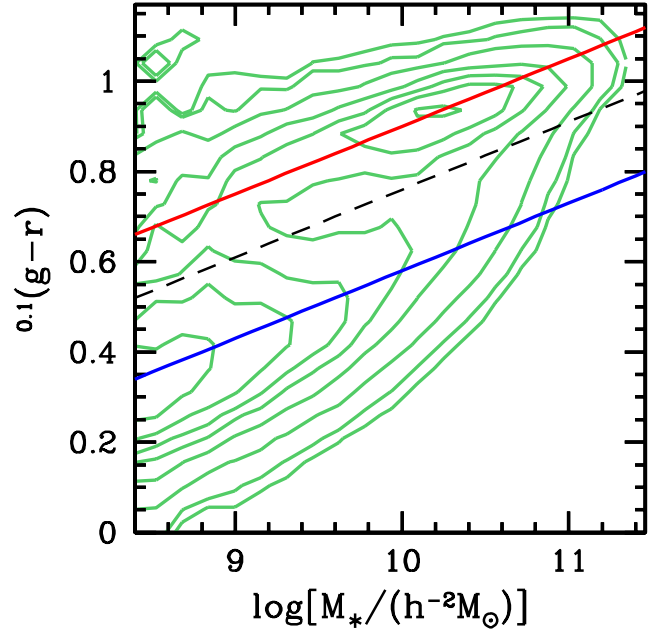


Figure 7. Contour plot of the $1/V_{\text{max}}$ -weighted distribution of galaxies in sample IIa as function of color and stellar mass. The red and blue lines indicate the red and blue sequences, respectively (fit by eye), while the dashed black line indicates our split in red (above) and blue (below) galaxies.

and blue galaxies, and is parameterized by eq. (1) with $0.1A = 0.1A_{\text{cut}} = 0.76$. Again, this cut is chosen somewhat arbitrarily, though our results are not sensitive to the exact value of $0.1A_{\text{cut}}$ adopted. Alternatively, we could have fitted the color distribution at various stellar mass bins with a bi-Gaussian function, and use the bisector of the medians of the two Gaussians to split the galaxy population in red and blue (cf. Baldry et al. 2004; Li et al. 2006). Although this is less ambiguous than our simple fit-by-eye, it has a problem in that the color-distribution is no-longer bimodal at $M_* \gtrsim 10^{11} h^{-2} M_\odot$. Consequently, the bisector basically splits the massive end of the red sequence in two. We therefore believe that our method for splitting the galaxy population in red and blue is more sensible.

Using the above color-cut and our group catalogue, we now investigate the importance of satellite-specific transformation processes for the build-up of the red sequence. In what follows, we use the subscripts ‘r’ and ‘b’ to refer to ‘red’ and ‘blue’, and the subscripts ‘c’ and ‘s’ to refer to ‘centrals’ and ‘satellites’, respectively. All fractions are properly weighted by $1/V_{\text{max}}$ to correct for Malmquist bias. For example, the fraction of satellites that are red is given by

$$f_{r|s}(M_*) = \sum_{i=1}^{N_{rs}} w_i / \sum_{i=1}^{N_s} w_i, \quad (2)$$

where N_{rs} is the number of red satellites of mass M_* , N_s is the corresponding number of satellites, and w_i is the $1/V_{\text{max}}$ weight of galaxy i . Note that $f_{r|s}$ should not be confused with $f_{rs} = \sum_{i=1}^{N_{rs}} w_i / \sum_{i=1}^{N_{\text{tot}}} w_i$, which is the fraction of *all* galaxies of mass M_* that are red satellites, or with $f_{s|r} = \sum_{i=1}^{N_{rs}} w_i / \sum_{i=1}^{N_r} w_i$, which is the satellite fraction of red galaxies (with N_r the total number of red galaxies of mass M_*). Errors are determined using the jackknife tech-

nique. We divide the group catalogue into $N = 20$ subsamples of roughly equal size, and recalculate the various fractions 20 times, each time leaving out one of the 20 subsamples. The jackknife estimate of the standard deviation then follows from

$$\sigma_f = \sqrt{\frac{N-1}{N} \sum_{i=1}^N (f_i - \bar{f})^2} \quad (3)$$

with f_i the fraction obtained from jackknife sample i , and \bar{f} is the average.

The black line in the upper left-hand panel of Fig. 8 shows the satellite fraction, f_s , as function of stellar mass. This decreases from ~ 0.35 at $M_* = 10^9 h^{-2} M_\odot$ to virtually zero at $M_* = 3 \times 10^{11} h^{-2} M_\odot$. The dashed (red) and dotted (blue) lines show the satellite fractions of red ($f_{s|r}$) and blue ($f_{s|b}$) galaxies, respectively. Clearly, the satellite fraction is higher for red galaxies than for blue galaxies. Note that these satellite fractions are in good agreement with results obtained from galaxy clustering (Cooray 2006; Tinker et al. 2007; van den Bosch et al. 2007) and from galaxy-galaxy lensing (Mandelbaum et al. 2006).

The upper right-hand panel of Fig. 8 plots the red fractions of central galaxies ($f_{r|c}$, solid line) and satellites ($f_{r|s}$, dashed line). In both cases the red fractions increase strongly with increasing stellar mass. Above $10^{11} h^{-2} M_\odot$ the red fractions of centrals and satellites are indistinguishable and close to unity. However, at the low mass end the red fractions are clearly higher for satellites than for centrals (see also Weinmann et al. 2006a). Under the assumption that present-day central galaxies are the progenitors of present-day satellite galaxies of the same stellar mass, this implies that a certain fraction of the satellite galaxies must have transited from the blue sequence to the red sequence as satellites. We now compute a number of different transition fractions. First we determine the fraction of all satellite galaxies that have undergone a blue sequence to red sequence transition after their accretion (i.e., after they became a satellite galaxy). This fraction is given by

$$f_{\text{tr}|s}(M_*) = f_{r|s}(M_*) - f_{r|c}(M_*) \quad (4)$$

and is shown as a solid line in the lower left-hand panel of Fig. 8. Note that $f_{\text{tr}|s}(M_*)$ drops from ~ 35 percent at $M_* \simeq 10^9 h^{-2} M_\odot$ to virtually zero for $M_* \gtrsim 10^{11} h^{-2} M_\odot$. However, this does not necessarily mean that the transformation process(es) work less efficiently on more massive galaxies. After all, only galaxies that are blue prior to becoming a satellite can undergo the blue-to-red transition. Therefore, the decrease of $f_{\text{tr}|s}$ with increasing stellar mass may also simply reflect that at the massive end most central galaxies are already on the red sequence. We can distinguish between these two different interpretations by examining the transition fraction of satellite galaxies that were still blue at the time of accretion. This transition fraction is given by

$$f_{\text{tr}|s,bc}(M_*) \equiv \frac{f_{\text{tr}|s}(M_*)}{f_{b|c}(M_*)} \quad (5)$$

and plotted as a dashed line in the lower left-hand panel of Fig. 8. Over the entire range in stellar masses probed, this transition fraction is remarkably constant at $f_{\text{tr}|s,bc} \simeq 0.4 \pm 0.1$. Thus, *satellite quenching affects roughly 40 percent*

of all galaxies that are still blue at their time of accretion, roughly independent of their stellar mass.

To express the overall impact of satellite quenching for the build-up of the red sequence, we now define the fraction of red sequence galaxies that arrived on the red sequence as a satellite galaxy. It is straightforward to show that this fraction is given by

$$f_{\text{tr}|r}(M_*) \equiv \frac{f_s(M_*) f_{\text{tr}|s}(M_*)}{f_r(M_*)} \quad (6)$$

and is shown as a solid line in the lower right-hand panel of Fig. 8. It rapidly drops from ~ 40 percent at $M_* = 10^9 h^{-2} M_\odot$ to ~ 10 percent at $M_* = 10^{10} h^{-2} M_\odot$ to zero for $M_* \gtrsim 10^{11} h^{-2} M_\odot$. This clearly demonstrates that the vast majority of all red sequence galaxies have undergone their blue sequence to red sequence transition as central galaxies; even at a stellar mass of $10^9 h^{-2} M_\odot$, less than half of the galaxies on the red sequence were quenched as a satellite galaxy. However, part of the reason why this transition fraction is so low is simply that the satellite fraction of (red) galaxies is relatively low. Therefore, we finally define the fraction of red sequence *satellite* galaxies that has undergone the blue sequence to red sequence transition as a satellite. This fraction is given by

$$f_{\text{tr}|rs}(M_*) \equiv \frac{f_s(M_*) f_{\text{tr}|s}(M_*)}{f_{rs}(M_*)} = \frac{f_{\text{tr}|s}(M_*)}{f_{r|s}(M_*)} \quad (7)$$

and shown as the dashed line in the lower right-hand panel of Fig. 8. Obviously this fraction is higher than $f_{\text{tr}|r}$, reaching ~ 70 percent at $M_* = 10^9 h^{-2} M_\odot$. Therefore, at this relatively low mass, only ~ 30 percent of the satellite galaxies on the red sequence had already been quenched before they became a satellite. At the massive end, however, this increases to virtually 100 percent.

We have verified that all four transition fractions defined above only depend very weakly on exactly how we split our sample in red and blue galaxies: increasing or decreasing $^{0.1}A_{\text{cut}}$ by 0.02 yields transition fractions that are almost indistinguishable from those shown in Fig. 8 within the errors.

Finally, as a consistency check, we compare the transition fractions derived here with the average color differences of matched central-satellite pairs presented in §3. The average color difference is related to the transition fraction according to

$$\begin{aligned} \langle ^{0.1}(g-r)_{\text{sat}} - ^{0.1}(g-r)_{\text{cen}} \rangle &\approx f_{\text{tr}|s} (^{0.1}A_{\text{red}} - ^{0.1}A_{\text{blue}}) \\ &\simeq 0.32 f_{\text{tr}|s} \end{aligned} \quad (8)$$

Comparing the lower left-hand panel of Fig. 8 with the upper panel in the middle column of Fig. 5 one can see that $f_{\text{tr}|s}(M_*)$ and $\langle ^{0.1}(g-r)_{\text{sat}} - ^{0.1}(g-r)_{\text{cen}} \rangle (M_*)$ are in excellent agreement with (8). For example, at $M_* \sim 3 \times 10^9 h^{-2} M_\odot$ the transition fraction of satellites is ~ 30 percent, which, according to (8), corresponds to an average color difference of ~ 0.1 magnitudes, in excellent agreement with the results shown in Fig. 5.

4.1 Caveats

There are a number of caveats with the above determination of the relative importance of satellite quenching. The

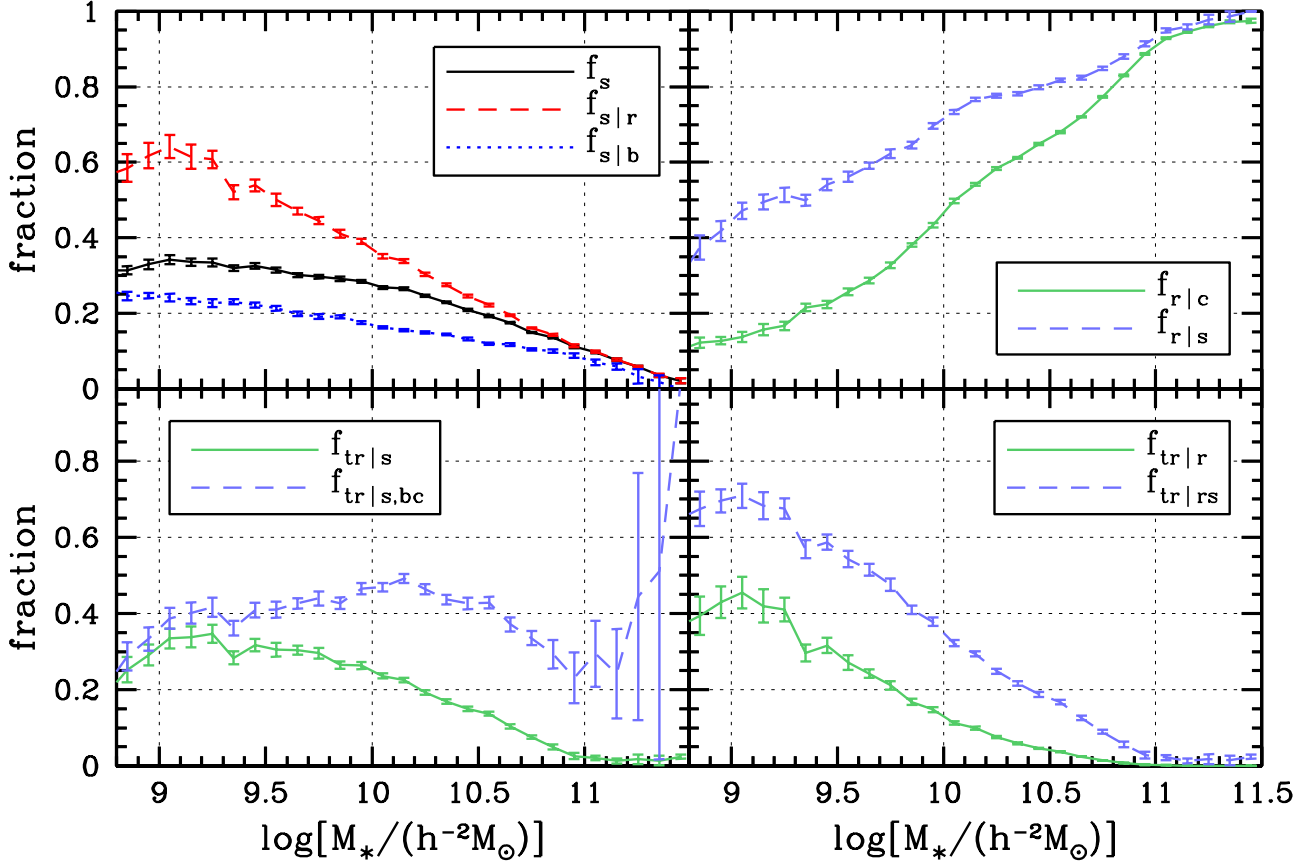


Figure 8. *Upper left:* The satellite fractions of all galaxies (f_s , solid black line), of red galaxies ($f_{s|r}$, dashed red line) and of blue galaxies ($f_{s|b}$, dotted blue line) as functions of stellar mass. *Upper right:* The red fractions of centrals ($f_{r|c}$, solid green line) and satellites ($f_{r|s}$, dashed blue line). Note that the fraction of red satellites is higher than that of red centrals, indicating that a certain fraction of galaxies has to transit to the red sequence once they become a satellite galaxy. *Lower left:* the transition fraction of satellites ($f_{tr|s}$, solid green line), and the transition fraction of satellites that were still blue at the time of accretion ($f_{tr|s,bc}$, solid green line). *Lower right:* the transition fraction of red sequence galaxies ($f_{tr|r}$, solid green line) and of red sequence satellites ($f_{tr|rs}$, dashed blue line). In all cases the errorbars are obtained using 20 jackknife samples. All fractions are $1/V_{\max}$ weighted, and are listed in Table 2.

main assumption that we have made is that the present day population of central galaxies can be considered representative of the progenitors of the present day satellite galaxies. However, in reality we should have compared the satellite galaxies to the population of central galaxies at the average redshift at which the satellites were accreted. Observations have shown that the mass density of galaxies on the red sequence has roughly doubled since $z \sim 1$ (see § 1). Therefore, the red fraction of centrals is probably lower at higher redshifts, which means that our estimates of the transition fractions are underestimated. However, we don't believe that this is a big effect. First of all, we have focused on relatively massive satellites, which most likely have only been accreted relatively recently, otherwise they would have merged with the central galaxy due to dynamical friction. This is in accord with the fact that the present day population of massive subhaloes (which host the massive satellite galaxies) fell into their parent halo fairly recently (Zentner & Bullock 2003; Gao et al. 2004; van den Bosch, Tormen & Giocoli 2005). Secondly, in Appendix A we use volume-limited subsamples that are complete in stellar mass to show that there is no significant indication for any evolution in the red frac-

tion of central galaxies over the redshift range covered here ($0.01 \leq z \leq 0.2$).

Another questionable assumption that we have (implicitly) made is that the galaxy preserves its stellar mass once it becomes a satellite galaxy. In reality, it may continue to form new stars (at least when it remains on the blue sequence) or it may lose stars due to tidal stripping. Since the latter is likely to dominate, one would need to compare the red fraction of satellites to the red fraction of centrals that are more massive, resulting in a lower transition fraction. To have some estimate of the magnitude of the effect of stripping, consider the case in which satellites have, on average, lost half their stellar mass since accretion. The transition fractions can then be computed comparing the red fraction of satellites at stellar mass M_* to the red fraction of centrals at $2M_*$. The resulting transition fractions are ~ 10 percent lower at the low mass end. At the massive end, however, this results in red fractions for the satellites that are *lower* than those of their central progenitors, resulting in negative transition fractions. We therefore argue that an average mass loss rate of 50 percent is a conservative upper limit and conclude that ignoring mass loss results in an overestimate of the various transition fractions of no more than 10 percent.

Table 2. Fractions

$\log(M_*)$ (1)	f_s (2)	$f_{s r}$ (3)	$f_{s b}$ (4)	$f_{r c}$ (5)	$f_{r s}$ (6)	$f_{tr s}$ (7)	$f_{tr s,bc}$ (8)	$f_{tr r}$ (9)	$f_{tr rs}$ (10)
8.85	31.4 ± 1.1	58.4 ± 3.7	24.6 ± 1.1	12.2 ± 1.4	37.4 ± 3.2	25.2 ± 3.4	28.7 ± 3.7	39.4 ± 5.0	67.5 ± 4.5
8.95	33.0 ± 1.3	61.8 ± 3.4	24.7 ± 0.7	12.7 ± 1.0	41.8 ± 2.6	29.1 ± 2.8	33.3 ± 3.1	43.0 ± 4.1	69.6 ± 3.0
9.05	34.2 ± 1.2	64.1 ± 3.1	24.2 ± 1.0	13.7 ± 1.3	47.1 ± 2.2	33.4 ± 2.6	38.7 ± 2.8	45.5 ± 4.1	70.9 ± 3.1
9.15	33.5 ± 1.0	61.5 ± 3.2	23.2 ± 0.8	15.7 ± 1.5	49.5 ± 2.0	33.8 ± 2.7	40.1 ± 2.8	42.0 ± 4.3	68.3 ± 3.5
9.25	33.4 ± 1.1	60.7 ± 2.3	22.7 ± 1.1	16.7 ± 1.2	51.3 ± 1.9	34.7 ± 2.4	41.6 ± 2.5	41.0 ± 3.1	67.6 ± 2.7
9.35	31.9 ± 0.8	52.1 ± 1.8	23.0 ± 0.7	21.5 ± 1.0	49.9 ± 1.4	28.4 ± 1.7	36.2 ± 2.0	29.6 ± 2.2	56.9 ± 2.4
9.45	32.5 ± 0.7	53.9 ± 1.6	22.2 ± 0.6	22.3 ± 1.0	54.1 ± 1.4	31.7 ± 1.6	40.9 ± 1.9	31.6 ± 1.9	58.7 ± 2.0
9.55	31.5 ± 0.7	50.1 ± 1.7	21.3 ± 0.6	25.7 ± 0.9	56.2 ± 1.4	30.5 ± 1.8	41.0 ± 2.1	27.2 ± 1.9	54.3 ± 2.2
9.65	30.1 ± 0.5	47.1 ± 0.9	19.8 ± 0.6	28.7 ± 0.7	59.1 ± 0.8	30.4 ± 1.2	42.6 ± 1.4	24.2 ± 1.1	51.5 ± 1.5
9.75	29.7 ± 0.5	44.6 ± 0.9	19.1 ± 0.6	32.7 ± 0.8	62.3 ± 1.2	29.6 ± 1.4	44.0 ± 1.9	21.2 ± 1.1	47.5 ± 1.6
9.85	29.1 ± 0.6	41.0 ± 1.0	19.0 ± 0.4	38.1 ± 0.4	64.5 ± 0.9	26.5 ± 1.0	42.7 ± 1.5	16.8 ± 0.8	41.0 ± 1.1
9.95	28.5 ± 0.4	39.1 ± 0.7	17.6 ± 0.4	43.3 ± 0.6	69.7 ± 0.7	26.4 ± 1.0	46.5 ± 1.4	14.8 ± 0.6	37.9 ± 1.1
10.05	26.9 ± 0.4	35.1 ± 0.6	16.3 ± 0.3	49.7 ± 0.6	73.3 ± 0.6	23.6 ± 0.7	47.0 ± 1.1	11.3 ± 0.5	32.2 ± 0.8
10.15	26.5 ± 0.4	33.8 ± 0.6	15.5 ± 0.3	54.1 ± 0.3	76.7 ± 0.5	22.5 ± 0.7	49.2 ± 1.2	9.9 ± 0.4	29.4 ± 0.7
10.25	24.7 ± 0.3	30.3 ± 0.5	14.9 ± 0.3	58.3 ± 0.3	77.7 ± 0.5	19.3 ± 0.6	46.4 ± 1.3	7.5 ± 0.3	24.9 ± 0.7
10.35	22.9 ± 0.2	27.5 ± 0.4	14.3 ± 0.2	61.2 ± 0.2	78.1 ± 0.4	16.9 ± 0.5	43.6 ± 1.3	6.0 ± 0.2	21.7 ± 0.6
10.45	20.9 ± 0.3	24.5 ± 0.4	13.1 ± 0.3	64.9 ± 0.3	79.9 ± 0.5	15.0 ± 0.6	42.7 ± 1.5	4.6 ± 0.2	18.8 ± 0.7
10.55	19.2 ± 0.3	22.2 ± 0.4	12.0 ± 0.3	68.0 ± 0.3	81.7 ± 0.5	13.7 ± 0.5	42.9 ± 1.5	3.7 ± 0.2	16.8 ± 0.6
10.65	17.5 ± 0.2	19.5 ± 0.2	11.7 ± 0.4	72.0 ± 0.2	82.4 ± 0.5	10.4 ± 0.5	37.1 ± 1.9	2.5 ± 0.1	12.6 ± 0.6
10.75	14.9 ± 0.2	16.1 ± 0.2	10.4 ± 0.3	77.3 ± 0.2	84.9 ± 0.4	7.6 ± 0.4	33.5 ± 1.9	1.4 ± 0.1	9.0 ± 0.5
10.85	13.6 ± 0.2	14.2 ± 0.3	10.0 ± 0.4	83.0 ± 0.2	88.0 ± 0.6	5.0 ± 0.7	29.3 ± 3.8	0.8 ± 0.1	5.7 ± 0.7
10.95	11.1 ± 0.3	11.4 ± 0.4	8.7 ± 0.6	88.8 ± 0.2	91.4 ± 0.7	2.6 ± 0.8	23.1 ± 6.7	0.3 ± 0.1	2.8 ± 0.8
11.05	9.7 ± 0.3	9.9 ± 0.3	7.0 ± 0.7	92.9 ± 0.2	95.0 ± 0.6	2.1 ± 0.6	29.4 ± 8.6	0.2 ± 0.1	2.2 ± 0.7
11.15	7.6 ± 0.3	7.7 ± 0.3	5.9 ± 0.8	94.6 ± 0.2	95.9 ± 0.7	1.3 ± 0.6	24.2 ± 11.7	0.1 ± 0.1	1.4 ± 0.7
11.25	5.7 ± 0.3	5.8 ± 0.3	3.2 ± 1.9	96.1 ± 0.2	97.8 ± 1.3	1.7 ± 1.3	44.5 ± 32.4	0.1 ± 0.1	1.8 ± 1.3
11.35	3.5 ± 0.4	3.5 ± 0.4	1.7 ± 1.8	97.2 ± 0.4	98.6 ± 1.4	1.4 ± 1.3	51.1 ± 49.4	0.1 ± 0.0	1.5 ± 1.2
11.45	2.1 ± 0.6	2.1 ± 0.7	0.0 ± 0.0	97.5 ± 0.6	100.0 ± 0.0	2.5 ± 0.6	100.0 ± 0.0	0.1 ± 0.0	2.5 ± 0.6

Notes: Various (transition) fractions discussed in the text and shown in Fig. 8. Column (1) lists the 10-based logarithm of the stellar mass (in $h^{-2} M_\odot$), while columns (2) to (10) list the various fractions plus their jackknife errors (both multiplied by 100).

Finally, there is a potential problem concerning the impact of interlopers, which are galaxies assigned to a group that in reality reside in a different dark matter halo than the other group members. Although our group finding algorithm has been optimized to yield low interloper fractions (see Yang et al. 2005a and Y07), detailed tests with mock redshift surveys suggest that we still have an interloper fraction of roughly 15 ± 5 percent (see Fig. 2 in Yang et al. 2005a). Most of these interlopers are blue centrals in low mass haloes which have been erroneously identified as a group member (satellite) of a bigger halo along the line of sight to the observer. Thus, interlopers tend to result in an overestimate of the blue fraction of satellites, and hence in an underestimate of the relative importance of satellite quenching. Since not all interlopers are blue, though, we estimate that the presence of interlopers may cause us to underestimate the transition fractions, $f_{tr|s}$, by no more than 10 percent.

To summarize, we have argued that the three effects mentioned here, evolution, mass loss and interlopers, all have only a modest effect on the inferred transition fractions. Furthermore, since ignoring mass loss results in an overestimate while ignoring evolution and interlopers results in an underestimate, the cumulative effect is likely to be small. Nevertheless, it is clear that potential systematic errors can be significantly larger than the random (jackknife) errors adopted here. We intend to address these issues in a forthcoming paper using large mock redshift surveys based on a semi-analytical model for galaxy formation.

5 CONCLUSIONS

We have used the SDSS group catalogue of Yang et al. (2007) to investigate the differences between centrals and satellites of the same stellar mass. Under the hypothesis that a satellite galaxy was a central galaxy of the same stellar mass before it was accreted into its new host halo, this sheds light on the impact of the various transformation mechanisms that are believed to operate on satellite galaxies. Our conclusions can be summarized as follows:

- On average, satellite galaxies reside in dark matter haloes that are roughly twenty times more massive than central galaxies of the same stellar mass.
- On average, satellites are somewhat redder and slightly more concentrated than central galaxies of the same stellar mass. There is a clear stellar mass dependence, in the sense that the color and concentration differences are larger for less massive central-satellite pairs. In fact, satellites with $M_* \gtrsim 10^{11} h^{-2} M_\odot$ have average colors and concentrations that are almost identical to those of central galaxies of the same stellar mass. This does not imply, though, that the transformation processes are less efficient for more massive galaxies. Rather, it simply reflects that virtually all galaxies with $M_* \gtrsim 10^{11} h^{-2} M_\odot$ are already red at the time they are accreted into a larger halo. Massive galaxies, therefore, must have undergone their late-to-early type transition while they were still a central galaxy, most likely due to the impact of a major merger.

- Central-satellite pairs that are matched in both stellar mass and color show no differences in concentration. However, pairs that are matched in both stellar mass and concentration show significant color differences, at least for $M_* \lesssim 10^{11} h^{-2} M_\odot$. This suggests that strangulation and/or ram-pressure stripping, which affect the color, but not the concentration, of a galaxy are more efficient than transformation mechanisms that have a strong impact on the galaxy's morphology, such as harassment.

- The average color and concentration differences of central-satellite pairs that are matched in stellar mass are independent of the halo mass of the satellite. This indicates that the transformation mechanism(s) that operate on the satellite galaxies are equally efficient in haloes of all masses. This in turn argues against transformation mechanisms that are thought to operate only in very massive haloes, such as ram-pressure stripping or harassment. Although these processes do occur, they are not the dominant cause of satellite quenching.

- Comparing the blue fractions of centrals and satellites of the same stellar mass we infer that roughly 40 percent of the blue galaxies transit to the red sequence after having been accreted into a bigger halo (i.e., after having become a satellite galaxy). Since more massive galaxies are less likely to be blue at the time they are accreted, the fraction of *all* satellites that undergoes a transition (between their time of accretion and the present) decreases from ~ 35 percent at $M_* = 10^9 h^{-2} M_\odot$ to basically zero percent at $M_* = 10^{11} h^{-2} M_\odot$.

- Roughly 70 percent of satellite galaxies with $M_* = 10^9 h^{-2} M_\odot$ that are on the red sequence at the present have undergone satellite quenching. The remaining 30 percent were already red at their time of accretion (i.e., when they became a satellite galaxy). For more massive satellites, this relative importance of satellite quenching is much lower. For example, only ~ 35 percent of the red sequence satellite galaxies with $M_* = 10^{10} h^{-2} M_\odot$ have experienced satellite quenching, while ~ 65 percent were already red at accretion. At $M_* = 10^{11} h^{-2} M_\odot$ virtually all satellites were already red at accretion.

These results are most consistent with a picture in which strangulation is the main mechanism that operates on satellite galaxies, and that causes their transition from the blue to the red sequence. This conclusion is consistent (i) with indications that star formation quenching takes place on relatively long time scales (Kauffmann et al. 2004), (ii) with the dependence of the blue and red fractions on halo mass and galaxy luminosity (Weinmann et al. 2006a), (iii) with recent simulation results (Kawata & Mulchaey 2007), and (iv) with a number of recent studies that found that star formation quenching cannot be ascribed solely to processes that are significant only in rich clusters, such as ram-pressure stripping and galaxy harassment (e.g., Balogh et al. 2002; Tanaka et al. 2004; Cooper et al. 2007; Gerke et al. 2007; Verdugo, Ziegler & Gerken 2007).

An important, outstanding question regards the morphological transformations. Since most red sequence galaxies are spheroids, while most blue sequence galaxies are disks, it is clear that quenching alone cannot explain the build-up of the red-sequence; an additional mechanism is required to transform the disks into spheroids. We emphasize, there-

fore, that strangulation is the main, not the *only*, transformation mechanism operating on satellite galaxies. Ram-pressure stripping, harassment, tidal stripping and heating, and even satellite-satellite mergers almost certainly occur as well. After all, as we have shown, satellites are slightly more concentrated than centrals of the same stellar mass, indicating that satellites on average undergo a mild change in morphology. Since strangulation only results in a quenching of the star formation, additional mechanisms are required to explain the full set of data. If we make the simple assumption that those galaxies that are already red at the time of accretion are spheroids (since their transformation mechanism is most likely related to a major merger), while the red sequence galaxies that are quenched as satellites maintain their disk morphology, we can use the results presented in §4 to predict the spheroid fraction of red sequence galaxies as function of stellar mass: it should simply be $1 - f_{\text{tr}|r}$, and thus range from unity for $M_* \gtrsim 10^{11} h^{-2} M_\odot$ to ~ 60 percent at $M_* = 10^9 h^{-2} M_\odot$. Any significant deviations from this simple prediction most likely reflect the impact of the additional satellite-specific transformation processes. We intend to investigate the morphological make-up of the red-sequence (as function of stellar mass) in a forthcoming study.

In most semi-analytical models for galaxy formation (e.g., Kauffmann, White & Guiderdoni 1993; Somerville & Primack 1999; Cole et al. 2000; Croton et al. 2006; Kang et al. 2006) strangulation is included (while most of the other processes, such as ram-pressure stripping, tidal heating and harassment are not). However, as shown by Weinmann et al. (2006b) and Baldry et al. (2006), the semi-analytical models still predict a red fraction for satellites that is much too high (see Coil et al. 2007 for a similar discrepancy at $z \sim 1$). It is unclear at the present whether this is due to strangulation being modeled too efficiently, or whether it reflects a problem with the colors of the infalling population. In all semi-analytical models strangulation is modeled by instantaneously removing the entire hot-gas reservoir of a galaxy as soon as it becomes a satellite. However, recently McCarthy et al. (2007) have performed a large suite of hydrodynamical simulations and shown that $\sim 30\%$ of the hot gas associated with a satellite galaxy remains bound to its subhalo for as long as 10 Gyr. This implies that the satellites can continue to form stars for a longer period (as long as the hot gas in the subhalo can cool), resulting in a less efficient quenching of the star formation (see also Kawata & Mulchaey 2007). It remains to be seen whether a more realistic description of strangulation, consistent with these simulation results, can successfully fit the data presented here. In this respect, including similar constraints from higher redshifts, such as those provided by Cooper et al. (2006), Cucciati et al. (2006) and Gerke et al. (2007), will prove extremely useful to further our understanding of the build-up of the red sequence.

ACKNOWLEDGMENTS

FvdB thanks the Aspen Center for Physics where part of this work has been done, and is grateful to Eric Bell, Andreas Berlind, Alison Coil, Charlie Conroy, Hans-Walter Rix, Erin Sheldon, Jeremy Tinker, Risa Wechsler and Si-

mon White for enlightening discussions. DHM acknowledges support from the National Aeronautics and Space Administration (NASA) under LTSA Grant NAG5-13102 issued through the Office of Space Science.

REFERENCES

- Adelman-McCarthy J.K., et al., 2006, *ApJS*, 162, 38
- Baldry I.K., Glazebrook K., Brinkmann J., Ivezić Z., Lupton R.H., Nichol R.C., Szalay A.S., 2004, *ApJ*, 600, 681
- Baldry I.K., Balogh M.L., Bower R.G., Glazebrook K., Nichol R.C., Bamford S.P., Budavari T., 2006, *MNRAS*, 373, 469
- Balogh M.L., Morris S.L., 2000, *MNRAS*, 318, 703
- Balogh M.L., Navarro J.F., Morris S.L., 2000, *ApJ*, 540, 113
- Balogh M.L., Bower R.G., Smail I., Ziegler B.L., Davies R.L., Gaztela A., Alexander F., 2002, *MNRAS*, 337, 256
- Bell E.F., McIntosh D.H., Katz N., Weinberg M.D., 2003, *ApJS*, 149, 289
- Bell E.F., et al., 2004, *ApJ*, 608, 752
- Blanton M.R. et al., 2003, *ApJ*, 592, 819
- Blanton M.R. et al., 2005a, *AJ*, 129, 2562
- Blanton M.R., Eisenstein D., Hogg D.W., Schlegel D.J., Brinkmann J., 2005b, *ApJ*, 629, 143
- Blanton M.R., Roweis S., 2007, *AJ*, 133, 734
- Borch A., et al., 2006, *A&A*, 453, 869
- Bower R.G., 2006, *MNRAS*, 370, 645
- Brown M.J.I., Dey A., Jannuzi B.T., Brand K., Benson A.J., Brodwin M., Croton D.J., Eisenhardt P.R., 2007, *ApJ*, 654, 858
- Coil A., et al., 2007, preprint (arXiv:0708.0004)
- Cole S., Lacey C.G., Baugh C.M., Frenk C.S., 2000, *MNRAS*, 319, 168
- Cooper M.C., et al., 2006, *MNRAS*, 370, 198
- Cooper M.C., et al., 2007, *MNRAS*, 376, 1445
- Cooray A., 2006, *MNRAS*, 365, 842
- Croton D.J., et al., 2006, *MNRAS*, 356, 1155
- Cucciati O., et al., 2006, *A&A*, 458, 39
- Faber S.M., et al., 2007, *ApJ*, 665, 265
- Farouki R., Shapiro S.L., 1981, *ApJ*, 243, 32
- Gao L., White S.D.M., Jenkins A., Stoehr F., Springel V., 2004, *MNRAS*, 355, 899
- Gerke B.F., et al., 2007, *MNRAS*, 376, 1425
- Gunn J.E., Gott J.R., 1972, *ApJ*, 176, 1
- Hester J.A., 2006a, *ApJ*, 647, 910
- Hester J.A., 2006b, preprint (astro-ph/0610089)
- Hopkins P.F., Hernquist L., Cox T.J., DiMatteo T., Robertson B., Springel V., 2006, *ApJS*, 163, 1
- Hopkins P.F., Hernquist L., Cox T.J., Keres D., 2007a, preprint (arXiv:0706.1243)
- Hopkins P.F., Cox T.J., Keres D., Hernquist L., 2007b, preprint (arXiv:0706.1246)
- Hogg D.W., et al., 2003, *ApJ*, 585, L5
- Kang X., Jing Y.P., Silk J., 2006, *ApJ*, 648, 820
- Kauffmann G., White S.D.M., Guiderdoni B., 1993, *MNRAS*, 264, 201
- Kauffmann G., White S.D.M., Heckman T.M., Ménard, Brinchmann J., Charlot S., Tremonti C., Brinkmann J., 2004, *MNRAS*, 353, 713
- Kawata D., Mulchaey J.S., 2007, preprint (arXiv:0707.3814)
- Larson R.B., Tinsley B.M., Caldwell C.N., 1980, *ApJ*, 237, 692
- Li C., Kauffmann G., Jing Y.P., White S.D.M., Börner G., Cheng F.Z., 2006, *MNRAS*, 358, 21
- Makino J., Hut P., 1997, *ApJ*, 481, 83
- Mandelbaum R., Seljak U., Kauffmann G., Hirata C.M., Brinkmann J., 2006, *MNRAS*, 368, 715
- McCarthy I.G., Frenk C.S., Font A.S., Lacey C.C., Bower R.G., Mitchell N.L., Balogh M.L., Theuns T., 2007, preprint (arXiv:0710.0964)
- McIntosh D.H., Guo Y., Hertzberg J., Katz N., Mo H.J., van den Bosch F.C., Yang X., 2007, preprint (arXiv:0710.2157)
- Moore B., Katz N., Lake G., Dressler A., Oemler A., 1996, *Nature*, 379, 613
- Negroponte J., White S.D.M., 1983, *MNRAS*, 205, 1009
- Petrosian V., 1976, *ApJ*, 209, L1
- Quilis V., Moore B., Bower R., 2000, *science*, 288, 1617
- Schlegel D.J., Finkbeiner D.P., Davis M., 1998, *ApJ*, 500, 525
- Somerville R.S., Primack J.R., 1999, *MNRAS*, 310, 1087
- Spergel D.N., et al., 2007, *ApJS*, 170, 377
- Stoughton C., et al., 2002, *AJ*, 123, 485
- Strateva I., et al., 2001, *ApJ*, 122, 1861
- Strauss M.A., et al., 2002, *AJ*, 124, 1810
- Tanaka M., Goto T., Okamura S., Shimasaku K., Brinkman J., 2004, *AJ*, 128, 2677
- Tanaka M., Kodama T., Arimoto N., Okamura S., Umetsu K., Shimasaku K., Tanaka I., Yamada T., 2005, *MNRAS*, 362, 268
- Tinker J.L., Norberg P., Weinberg D.H., Warren M.S., 2007, *ApJ*, 659, 877
- Toomre A., Toomre J., 1972, *ApJ*, 178, 623
- van den Bosch F.C., Tormen G., Giocoli C., 2005, *MNRAS*, 359, 1029
- van den Bosch F.C., et al., 2007, *MNRAS*, 376, 841
- Verdugo M., Ziegler B.L., Gerken B., 2007, preprint (arXiv:0709.4508)
- Weinmann S.M., van den Bosch F.C., Yang X., Mo H.J., 2006a, *MNRAS*, 366, 2
- Weinmann S.M., van den Bosch F.C., Yang X., Mo H.J., Croton D.J., Moore B., 2006b, *MNRAS*, 372, 1161
- Willmer C., et al., 2006, *ApJ*, 647, 853
- Yang X., Mo H.J., van den Bosch F.C., Jing Y.P., 2005a, *MNRAS*, 356, 1293
- Yang X., Mo H.J., van den Bosch F.C., Jing Y.P., 2005b, *MNRAS*, 357, 608
- Yang X., Mo H.J., van den Bosch F.C., Pasquali A., Li C., Barden M., 2007, *MNRAS*, in press (arXiv:0707.4640)
- York D.G., et al., 2000, *AJ*, 120, 1579
- Zehavi I., et al., 2002, *ApJ*, 571, 172
- Zentner A.R., Bullock J.S., 2003, *ApJ*, 589, 49
- Zucca E., et al., 2006, *A&A*, 455, 879

APPENDIX A: REDSHIFT EVOLUTION

Here we illustrate how the apparent magnitude limit of the SDSS results in a stellar mass limit that depends on both redshift and color, and we describe the construction of volume-limited subsamples that are complete in stellar mass, and which we use to test for redshift evolution in the red fraction of centrals.

The upper left-hand panel of Fig. A1 shows the absolute magnitude-redshift relation covering the redshift range $0.01 \leq z \leq 0.2$. Galaxies are color coded according to whether they are red or blue (based on the definition of §4). The apparent magnitude limit of the sample ($m_r = 17.77$) translates into a redshift dependent absolute magnitude limit given by

$$^{0.1}M_{r,\text{lim}} - 5 \log h = 17.77 - \text{DM}(z) - k_{0.1}(z) + 1.62(z - 0.1). \quad (\text{A1})$$

where $k_{0.1}(z)$ is the K -correction to $z = 0.1$, the $1.62(z - 0.1)$ term is the evolution correction of Blanton et al. (2003), and

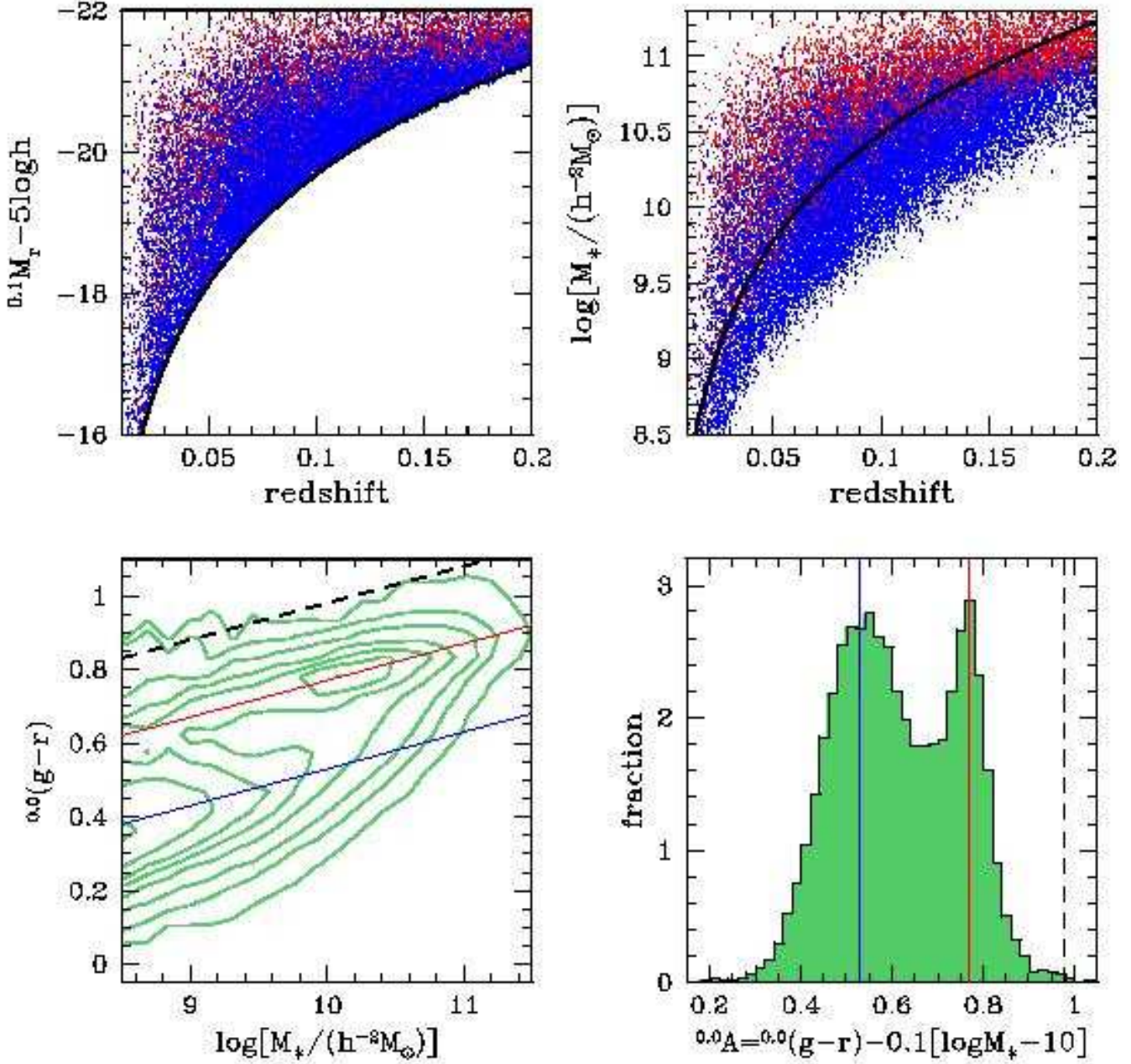


Figure A1. *Upper left-hand panel:* The distribution of galaxies in sample IIa as function of absolute $^{0.1}r$ -band magnitude and redshift (for clarity, only a random subsample of 10 percent of all galaxies is shown). Blue and red dots refer to blue and red galaxies, based on the criterion discussed in §4. Note that the $m_r = 17.77$ apparent magnitude limit of the sample results in a sharp, redshift dependent absolute magnitude limit. *Upper right-hand panel:* Same as the upper left-hand panel, except that we now plot the stellar mass as function of redshift. Note that blue galaxies (which have smaller stellar mass-to-light ratios) can be seen out to higher redshifts than red galaxies of the same stellar mass. The thick, black line indicates the stellar mass limit of eq. (A8) above which the sample is complete in stellar mass. *Lower left-hand panel:* Contours show the $1/V_{\max}$ weighted color-stellar mass distribution of SDSS galaxies. Contrary to Fig. 7 we here use the $^{0.0}(g-r)$ color, which is used to determine the stellar masses of the galaxies according to eq. (A4). The red and blue solid lines indicate the red and blue sequences, respectively, while the dashed line indicates our adopted upper envelope of the color-distribution. *Lower right-hand panel:* The $1/V_{\max}$ weighted distribution of $^{0.0}A$ for galaxies in our sample. The values of $^{0.0}A_{\text{red}}$, $^{0.0}A_{\text{blue}}$ and $^{0.0}A_{\text{lim}}$ are indicated with red, blue and dashed vertical lines, respectively. Note the pronounced bimodality, and that the red sequence is significantly narrower than the blue sequence.

$$DM(z) = 5 \log D_L(z) + 25 \quad (\text{A2})$$

is the distance measure corresponding to redshift z , with $D_L(z)$ the luminosity distance in h^{-1} Mpc. As discussed in §2, we have used the K -corrections of Blanton et al. (2003; see also Blanton & Roweis 2007), which are obtained using the five-band photometry of the SDSS. The redshift dependence is reasonably well described by

$$k_{0.1}(z) = 2.5 \log \left(\frac{z + 0.9}{1.1} \right) \quad (\text{A3})$$

Substituting this in (A1) yields the solid black line shown in the upper left-hand panel of Fig. A1. At $z = 0.1$, where (by definition) $k_{0.1} = -2.5 \log(1.1) \simeq -0.1$ for all galaxies (e.g., Blanton & Roweis 2007), this exactly gives the absolute magnitude limit of the sample. At lower and higher redshifts, however, a small fraction of the sample galaxies fall below this limit. This owes to the fact that $k_{0.1}(z)$ not only depends on redshift but also on color. For the analyses in this paper, however, this effect can safely be ignored.

As described in Y07, stellar masses for all galaxies in our sample have been computed using

$$\log[M_*/(h^{-2} M_\odot)] = -0.406 + 1.097 \left[{}^{0.0}(g-r) \right] - 0.4 \left({}^{0.0}M_r - 5 \log h - 4.64 \right), \quad (\text{A4})$$

(see Bell et al. 2003), where ${}^{0.0}M_r - 5 \log h$ is the absolute magnitude K -corrected and evolution corrected to $z = 0.0$ using

$${}^{0.0}M_r - 5 \log h = m_r - DM(z) - k_{0.0}(z) + 1.62z. \quad (\text{A5})$$

The upper right-hand panel of Fig. A1 shows the resulting stellar mass as function of redshift, using the same color coding as in the upper left-hand panel. Note that there is no sharp limit to the stellar mass distribution at any given redshift, and that the low mass end is entirely dominated by blue galaxies. This arises because blue galaxies have a lower stellar mass-to-light ratio than red galaxies of the same stellar mass, which is expressed by the color-term in (A4). Therefore, in a flux-limited sample, blue galaxies can be seen out to higher redshifts than red galaxies *of the same stellar mass*. In the analysis described in §4 this bias has been corrected for by weighting all galaxies by $1/V_{\max}$ when computing red and blue fractions.

To construct volume-limited subsamples that are complete in stellar mass, we proceed as follows. Since redder galaxies have higher stellar mass-to-light ratios, we first determine a suitable upper limit to the color distribution of galaxies as function of their stellar mass. The lower left-hand panel of Fig. A1 shows a contour plot of the $1/V_{\max}$ weighted distribution of galaxies in the parameter space of ${}^{0.0}(g-r)$ versus stellar mass. Similar to Fig. 7, it clearly reveals the bimodal color distribution of the galaxy distribution. Fitting the stellar mass dependence of the red and blue sequences (by eye) we obtain

$${}^{0.0}(g-r) = {}^{0.0}A + 0.10 \left(\log[M_*/(h^{-2} M_\odot)] - 10.0 \right), \quad (\text{A6})$$

with ${}^{0.0}A = {}^{0.0}A_{\text{red}} = 0.77$ and ${}^{0.0}A = {}^{0.0}A_{\text{blue}} = 0.54$ for the red and blue sequences, respectively. The dashed line corresponds to ${}^{0.0}A = {}^{0.0}A_{\text{lim}} = 0.98$ and roughly reflects the upper limit to the color distribution (only 0.3 per cent of the galaxies in our sample have colors redder than this). This is further illustrated in the lower right-hand panel

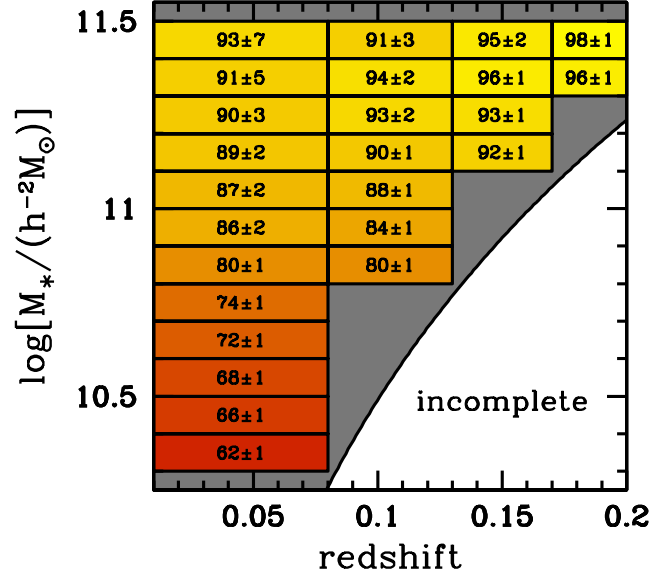


Figure A2. Redshift and stellar mass dependence of the red fraction of centrals. The gray area indicates the parameter space where we are complete in stellar mass (i.e., the region above $M_{*,\text{lim}}(z)$ given by eq. [A8]), and the shaded boxes indicate volume-limited subsamples that are complete in stellar mass. They are color coded according to their red fraction of centrals, the value and (Poisson) error of which are indicated. Note that there is no significant indication of redshift evolution.

of Fig. A1 which plots the $1/V_{\max}$ -weighted distribution of ${}^{0.0}A = {}^{0.0}(g-r) - 0.10 \left(\log[M_*/(h^{-2} M_\odot)] - 10.0 \right)$ for all galaxies in our sample. Note that the bi-modality of the color distribution is now extremely clear, as is the fact that the red sequence is significantly narrower than the blue sequence.

The final ingredient required for the construction of volume limited sub-samples that are complete in stellar mass is a simple fitting function for $k_{0.0}(z)$. After some experimenting we found that the color and redshift dependence of $k_{0.0}(z)$ can be reasonably well described by

$$k_{0.0}(z) = 2.5 \log(1.0 + z) + 1.5z \left[{}^{0.0}(g-r) - 0.66 \right] \quad (\text{A7})$$

Combining (A4)-(A7) and adopting $m_r = 17.77$ and ${}^{0.0}A = 0.98$, we obtain a relation between stellar mass and redshift given by

$$\log[M_{*,\text{lim}}/(h^{-2} M_\odot)] = \frac{4.852 + 2.246 \log D_L(z) + 1.123 \log(1+z) - 1.186z}{1 - 0.067z} \quad (\text{A8})$$

and indicated by the thick, solid line in the upper right-hand panel of Fig. A1. We can now define volume-limited subsamples that are complete in stellar mass, by only selecting galaxies that lie above this limit. The shaded boxes in Fig. A2 indicate such samples. The boxes are color-coded according to their red fraction of centrals, $f_{r|c}$, the value and (Poisson) error of which are indicated. Note that within the errors there is no indication for any significant redshift evolution in $f_{r|c}$, though it is clear that the redshift-dependent stellar mass limit of eq. (A8) only allows us to investigate this for the most massive centrals.